

AFRL-RV-HA-TR-2009-1100

Comprehensive Methods for Determining Space Effects on Air Force Systems

**Patricia H. Doherty
Anthony J. Midey
Thomas M. Miller
Dale J. Levandier
Ernest Holeman
David F. Webb
Kevin Martin**

**Boston College
Institute for Scientific Research
140 Commonwealth Avenue
Chestnut Hill, MA 02467**

Final Report

4 August 2009

APPROVED FOR PUBLIC RELEASE; DISTRIBUTION IS UNLIMITED.



**AIR FORCE RESEARCH LABORATORY
Space Vehicles Directorate
29 Randolph Rd.
AIR FORCE MATERIEL COMMAND
Hanscom AFB, MA 01731-3010**

DTIC COPY

AFRL-RV-HA-TR-2009-1100

Using Government drawings, specifications, or other data included in this document for any purpose other than Government procurement does not in any way obligate the U.S. Government. The fact that the Government formulated or supplied the drawings, specifications, or other data, does not license the holder or any other person or corporation; or convey any rights or permission to manufacture, use, or sell any patented invention that may relate to them.

This report is published in the interest of scientific and technical information exchange and its publication does not constitute the Government's approval or disapproval of its ideas or findings.

This technical report has been reviewed and is approved for publication.

/ signed /
Alan D. Rebello
Contract Manager

/ signed /
Dwight T. Decker, Chief
Space Weather Center of Excellence

This report has been reviewed by the ESC Public Affairs Office (PA) and is releasable to the National Technical Information Service (NTIS).

Qualified requestors may obtain additional copies from the Defense Technical Information Center (DTIC). All other requestors should apply to the National Technical Information Service (NTIS).

If your address has changed, if you wish to be removed from the mailing list, or if the addressee is no longer employed by your organization, please notify AFRL/RVIM, 29 Randolph Road, Hanscom AFB, MA 01731-3010. This will assist us in maintaining a current mailing list.

Do not return copies of this report unless contractual obligations or notices on a specific document require that it be returned.

REPORT DOCUMENTATION PAGEForm Approved
OMB No. 0704-0188

Public reporting burden for this collection of information is estimated to average 1 hour per response, including the time for reviewing instructions, searching existing data sources, gathering and maintaining the data needed, and completing and reviewing this collection of information. Send comments regarding this burden estimate or any other aspect of this collection of information, including suggestions for reducing this burden to Department of Defense, Washington Headquarters Services, Directorate for Information Operations and Reports (0704-0188), 1215 Jefferson Davis Highway, Suite 1204, Arlington, VA 22202-4302. Respondents should be aware that notwithstanding any other provision of law, no person shall be subject to any penalty for failing to comply with a collection of information if it does not display a currently valid OMB control number. PLEASE DO NOT RETURN YOUR FORM TO THE ABOVE ADDRESS.

1. REPORT DATE (DD-MM-YYYY) 04-08-2009		2. REPORT TYPE Scientific Report - Final		3. DATES COVERED (From - To) 05-05-2004 to 04-05-2009	
4. TITLE AND SUBTITLE Comprehensive Methods for Determining Space Effects on Air Force Systems				5a. CONTRACT NUMBER FA8718-04-C-0006	
				5b. GRANT NUMBER	
				5c. PROGRAM ELEMENT NUMBER 63401F	
6. AUTHOR(S) P.H. Doherty, A.J. Midey, T.J. Miller, D.J. Levandier, E. Holeman, D.F. Webb, Kevin Martin				5d. PROJECT NUMBER 5021	
				5e. TASK NUMBER RD	
				5f. WORK UNIT NUMBER A1	
7. PERFORMING ORGANIZATION NAME(S) AND ADDRESS(ES) Boston College Institute for Scientific Research 140 Commonwealth Avenue Chestnut Hill, MA 02467				8. PERFORMING ORGANIZATION REPORT NUMBER	
9. SPONSORING / MONITORING AGENCY NAME(S) AND ADDRESS(ES) Air Force Research Laboratory 29 Randolph Rd. Hanscom AFB, MA 01731-3010				10. SPONSOR/MONITOR'S ACRONYM(S) AFRL/RVBXT	
				11. SPONSOR/MONITOR'S REPORT NUMBER(S) AFRL-RV-HA-TR-2009-1100	

12. DISTRIBUTION / AVAILABILITY STATEMENT

Approved for Public Release; Distribution Unlimited.

13. SUPPLEMENTARY NOTES**20100405185****14. ABSTRACT**

The Boston College Institute for Scientific Research has performed innovative research and analysis to increase the knowledge of space effects on Air Force systems. Sections in this report address a wide range of efforts from applying chemical techniques to the development of new technologies for Air Force space-based systems to developing a database of various measurements made by the Defense Meteorological Satellite Program (DMSP). In addition, our research explored solar and interplanetary disturbances and their coupling to geomagnetic storms. Another study involved research and development of highly miniaturized satellite skin sensor technology capable of measuring ionospheric neutral particles. This real-time, in-situ capability enables distributed, remote density measurements via small satellites including the Air Force C/NOFS (Communications/Navigation Outage Forecast System) satellite mission. All aspects of the research process were included in our efforts. From data acquisition, analysis, theoretical explanation, database development to summary of our efforts. Much of our work was published in peer reviewed journals as evidenced in Section 7 with more than 45 publications over the course of this contract.

15. SUBJECT TERMS

Ionosphere, Plasma chemistry, Kinetic studies, Space chemistry, DMSP, SMEI

16. SECURITY CLASSIFICATION OF:

a. REPORT UNCLASSIFIED	b. ABSTRACT UNCLASSIFIED	c. THIS PAGE UNCLASSIFIED
----------------------------------	------------------------------------	-------------------------------------

17. LIMITATION OF ABSTRACT

SAR

18. NUMB

24

19a. NAME OF RESPONSIBLE PERSON**19b. TELEPHONE NUMBER (include area code)**

781-377-9669

Table of Contents

	Page
1. INTRODUCTION.....	1
2. CHEMICAL PROCESSES.....	1
2.1. Kinetics Studies of a Variety of Positive and Negative Ions.....	2
2.2. Kinetics of Ion-Molecule Reactions.....	2
2.3. Reaction Kinetics of PO ₂ Cl ⁺ , POCl ₂ ⁺ , and POCl ₃ ⁺ with O ₂ and O ₃	3
2.4. Electron Attachment to SF ₅ X Compounds.....	3
2.5. Acidity of a Nucleotide Base.....	3
2.6. Electron Attachment to Cl ₂ from 300 to 1100 K.....	4
2.7. Electron Attachment and Detachment.....	4
2.8. Strong Emission from CaO in the 500 to 900 nm Region.....	5
3. SPACE CHEMISTRY.....	7
3.1. A Guided-Ion Beam Study of the O ⁺ (⁴ S) + NH ₃ System.....	8
3.2. Reactions of O ⁺ with C _n H _{2n+2} , n=2-4: A Guided Ion Beam Study.....	8
3.3. Hyperthermal Reactions of O ⁺ (⁴ S _{3/2}) with CD ₄ and CH ₄	9
4. SMEI SUPPORT AND INTERPLANETARY RESEARCH.....	9
4.1. Major Geomagnetic Storms.....	9
4.2. Solar Mass Ejection (SMEI) Observations of CMEs.....	10
5. DEFENSE METEOROLOGICAL SATELLITE PROGRAM (DMSP).....	10
5.1. DMSP Data Base Development.....	10
5.1.1. RSDR SSIES2 Phase II Processing.....	12
5.1.2. RSDR SSIES2 and SSIES3 Phase II EDR Processing.....	12
5.1.3. RSDR SSM Phase II MPR Processing.....	12
5.1.4. DMSP 3 and SWX Web Survey Plot Files (SSIES, SSJ & SSM).....	12
5.1.5. Raw Sensor Data Record Files (RSDR).....	13
5.2. DMSP J4/J5 Data Management.....	13
5.3. DMSP J5 Calibration.....	14
5.4. DMSP Auroral Boundary Maintenance.....	14
5.5. CEASE I and II.....	14
REFERENCES.....	15
PUBLICATIONS.....	17

Figures

1. Emission Spectrum of Interest	6
2. Spectral Radiation for a Reentry Object at 25 km	7
3. CEASE Measurements from the TSX-5 Vehicle (July 2000 – July 2006).....	15

Tables

1. Spectroscopic Constants for CaO.....	6
2. Einstein Coefficients for $A^1\Sigma(v') \rightarrow X^1\Sigma(v'')$, μs^{-1}	7

1. INTRODUCTION

The Boston College Institute for Scientific Research has performed innovative research and analysis to increase the knowledge of space effects on Air Force systems. Sections in this report address a wide range of efforts from applying chemical techniques to the development of new technologies for Air Force space-based systems to developing a database of various measurements made by the Defense Meteorological Satellite Program (DMSP). In addition, our research explored solar and interplanetary disturbances and their coupling to geomagnetic storms. Another study involved research and development of highly miniaturized satellite skin sensor technology capable of measuring ionospheric neutral particles. This real-time, in-situ capability enables distributed, remote density measurements via small satellites including the Air Force C/NOFS (Communications/Navigation Outage Forecast System) satellite mission.

All aspects of the research process were included in our efforts. From data acquisition, analysis, theoretical explanation, database development to summary of our efforts. Much of our work was published in peer reviewed journals as evidenced in Section 7 with more than 45 publications over the course of this contract.

2. CHEMICAL PROCESSES

Research performed under this contract included experimental and theoretical studies conducted in the plasma chemistry and mass spectroscopy laboratories, located on-site at AFRL/RVBXT. Experiments included: the selected ion flow drift tube, the high temperature flowing afterglow, the turbulent ion flow tube and the flowing afterglow Langmuir probe. These are fast flow kinetics devices for measuring ion and electron kinetics over a wide range of temperatures and pressures.

The overall purpose of this research was to understand and mitigate the fundamental processes that affect a wide-variety of Air Force interests where plasmas play a prominent role, e.g. the ionosphere, reentry vehicles and combustion.

Data measured included ion-molecule reaction rate constants and branching ratios over extended temperatures and pressure ranges. Research efforts also included engineering and maintenance tasks to design, assemble and test the experimental apparatuses. This required routine cleaning, maintenance of the vacuum pumps, as well as, leak checking, plumbing gas lines, and repairing electronics. Instrument upgrades were performed as necessary. Near the initial phase of this contract, a new custom-made heating system was installed on the turbulent ion flow tube (TIFT) to ensure uniform heating over the length of the flow tube including better temperature measurement and monitoring.

This work also included the development, validation and application of modeling and simulation tools to predict plasma formation on Air Force reentry and hypersonic vehicles and to specify the impact of plasma on reentry signatures and communication/navigation systems.

All aspects of the research were supported including data acquisition, data analysis, equipment maintenance and upgrade designs. All data sets were delivered to AFRL as they became available. Results of our research were presented at national and international conferences and published in peer reviewed journals. Section 6.0 lists nearly 40 publications

that resulted from our efforts. Some of the more notable research results are summarized in the following sections.

2.1. Kinetics Studies of a Variety of Positive and Negative Ions

Kinetics studies of a variety of positive and negative ions reacting with the GX surrogate, dimethyl methylphosphonate (DMMP), were performed. All protonated species reacted rapidly, that is, at the collision limit. The protonated reactant ions created from neutrals with proton affinities (PAs) less than or equal to the PA for ammonia reacted exclusively by nondissociative proton transfer. Hydrated H_3O^+ ions also reacted rapidly by proton transfer, with 25% of the products from the second hydrate, $\text{H}_3\text{O}^+(\text{H}_2\text{O})_2$, forming the hydrated form of protonated DMMP. Both methylamine and triethylamine reacted exclusively by clustering. NO^+ also clustered with DMMP at about 70% of the collision rate constant. O^+ and O_2^+ formed a variety of products in reactions with DMMP, with O_2^+ forming the nondissociative charge transfer product about 50% of the time. On the other hand, many negative ions were less reactive, particularly, SF_5^- , SF_6^- , CO_3^- , and NO_3^- . However, F^- , O^- , and O_2^- all reacted rapidly to generate $m/z = 109$ amu anions ($\text{PO}_3\text{C}_2\text{H}_6^-$). In addition, product ions with $m/z = 122$ amu from H_2^+ loss to form H_2O were the dominant ions produced in the O^- reaction. NO_2^- underwent a slow association reaction with DMMP at 0.4 Torr. G3(MP2) calculations of the ion energetics properties of DMMP, sarin, and soman were also performed. The calculated ionization potentials, proton affinities, and fluoride affinities were consistent with the trends in the measured kinetics and product ion branching ratios. The experimental results coupled with the calculated ion energetics helped to predict which ion chemistry would be most useful for trace detection of the actual chemical agents.

2.2. Kinetics of Ion-Molecule Reactions

The rate constants and product ion branching ratios have been measured in a selected ion flow tube (SIFT) at 298 K for a variety of positive and negative ions reacting with 2-chloroethyl ethyl sulfide (2-CEES), a surrogate for mustard gas (HD). This series of experiments is designed to elucidate ion-molecule reactions that have large rate constants and produce unique product ions to guide the development of chemical ionization mass spectrometry (CIMS) detection methods for the chemical weapon agent using the surrogate instead. The negative ions typically used in CIMS instruments are essentially unreactive with 2-CEES, that is, SF_6^- , SF_4^- , CF_3O^- , and CO_3^- . A few negative ions such as NO_2^- and NO_3^- undergo three-body association to give a unique product ion, but the bimolecular rate constants are small in the SIFT. Positive ions typically react at the collisional limit, primarily by charge and proton transfer, some of which is dissociative. For ions with high proton binding energies, association with 2-CEES has also been observed. Many of these reactions produced ions with the 2-CEES intact, including the parent cation, the protonated cation, and clusters. G3(MP2) calculations of the thermochemical properties for 2-CEES and mustard have been performed, along with calculations of the structures for the observed product cations. Reacting a series of protonated neutral molecules with 2-CEES brackets the proton affinity (PA) to between 812 ($(\text{CH}_3)_2\text{CO}$) and 854 (NH_3) kJ mol^{-1} . G3(MP2) calculations give a PA for 2-CEES of 823 kJ mol^{-1} and a PA for mustard of 796 kJ mol^{-1} , indicating that the

present results for 2- CEES should be directly transferable to mustard to design a CIMS detection scheme.

2.3. Reaction Kinetics of PO_2Cl^- , PO_2Cl_2^- , POCl_2^- , and POCl_3^- with O_2 and O_3

Rate constants and product ion branching fractions for the gas-phase reactions of O_2 and O_3 with the anions (a) PO_2Cl^- , (b) POCl_3^- , (c) POCl_2^- , and (d) PO_2Cl_2^- were measured in a selected-ion flow tube (SIFT). The kinetics were measured at temperatures of 163–400 K and a He pressure of 0.4 Torr. Only PO_2Cl^- reacts with O_2 to a measurable extent, having $k(163\text{--}400\text{ K}) = 1.1 \times 10^{-8}(T/\text{K})^{-1.0}\text{ cm}^3\text{ molecule}^{-1}\text{ s}^{-1}$, while O_3 reacts with all of the anions except PO_2Cl_2^- . The fitted rate constant expressions for the O_3 reaction with anions a–c are as follows: $k_a(163\text{--}400\text{ K}) = 3.5 \times 10^{-6}(T/\text{K})^{-1.6}$, $k_b(163\text{--}400\text{ K}) = 4.0 \times 10^{-7}(T/\text{K})^{-1.2}$, and $k_c(163\text{--}400\text{ K}) = 3.7 \times 10^{-7}(T/\text{K})^{-1.4}\text{ cm}^3\text{ molecule}^{-1}\text{ s}^{-1}$. Calculations were performed at the G3 level of theory to obtain optimized geometries, energies, and electron affinities (EAs) of the reactant and product species, as well as to determine the reaction thermochemistry to help understand the experimental results. The PO_xCl_y^- anions that have lower electron binding energies (eBE) and higher spin multiplicities are more reactive. The doublets are more labile than the singlets. How the extra electron density is distributed in the anion does not predict the observed reactivity of the ion. The reactions of PO_2Cl^- with O_2 and O_3 yield predominantly PO_3^- and PO_4^- . The reaction of POCl_2^- with O_3 yields mostly Cl^- and PO_2Cl_2^- , while the POCl_3^- reaction with O_3 yields mostly O_3^- and PO_2Cl_2^- .

2.4. Electron Attachment to SF_5X Compounds

Rate constants and ion product channels have been measured for electron attachment to four SF_5 compounds, $\text{SF}_5\text{C}_6\text{H}_5$, $\text{SF}_5\text{C}_2\text{H}_3$, S_2F_{10} , and SF_5Br , and these data are compared to earlier results for SF_6 , SF_5Cl , and SF_5CF_3 . The present rate constants range over a factor of 600 in magnitude. Rate constants measured in this work at 300 K are $9.9 \pm 3.0 \times 10^{-8}$ ($\text{SF}_5\text{C}_6\text{H}_5$), $7.3 \pm 1.8 \times 10^{-9}$ ($\text{SF}_5\text{C}_2\text{H}_3$), $6.5 \pm 2.5 \times 10^{-10}$ (S_2F_{10}), and $3.8 \pm 2.0 \times 10^{-10}$ (SF_5Br), all in $\text{cm}^3\text{ s}^{-1}$ units. SF_5^- was the sole ionic product observed for 300–550 K, though in the case of S_2F_{10} it cannot be ascertained whether the minor SF_4^- and SF_6^- products observed in the mass spectra are due to attachment to S_2F_{10} or to impurities. G3(MP2) electronic structure calculations (G2 for SF_5Br) have been carried out for the neutrals and anions of these species, primarily to determine electron affinities and the energetics of possible attachment reaction channels. Electron affinities were calculated to be 0.88 ($\text{SF}_5\text{C}_6\text{H}_5$), 0.70 ($\text{SF}_5\text{C}_2\text{H}_3$), 2.95 (S_2F_{10}), and 2.73 eV (SF_5Br). An anticorrelation is found for the Arrhenius A -factor with exothermicity for SF_5^- production for the seven molecules listed above. The Arrhenius activation energy was found to be anticorrelated with the bond strength of the parent ion.

2.5. Acidity of a Nucleotide Base

Experiment and calculations are used to show that the gas-phase acidity of uracil is comparable to that of HCl. The gas-phase acidity of uracil (denoted here by U) was bracketed by proton-transfer measurements involving U and various reference acids (denoted here by A) of known gas-phase acidity. Rate constants for proton transfer from the reference acid A to the conjugate anion of uracil, $(\text{U-H})^-$, were measured in a selected-ion flow tube at 298 K.

Rate constants for proton transfer from U to ions (A-H)⁻ were measured at 467 K in a flowing-afterglow Langmuir probe apparatus. Here, (U-H) or (A-H) indicates a U or A molecule which is missing an H atom, respectively. The result is $\Delta H^{\circ}_{\text{acid}}(\text{uracil}) = 333 \pm 5 \text{ kcal mol}^{-1}$ and $\Delta G^{\circ}_{\text{acid}}(\text{uracil}) = 326 \pm 5 \text{ kcal mol}^{-1}$ at 298 K, which agrees with earlier work. Thermal electron attachment to uracil was found to be too slow to permit measurement of a rate constant, consistent with the gas-phase acidity given above. G3 and G3(MP2) calculations are reported for uracil, and for each of the (U-H) radicals and (U-H)⁻ ions that result from H or H⁺ loss from each of the four hydrogen sites of U (on the N1, N3, C5, and C6 positions). From the calculated total energies we obtain the gas-phase acidity of uracil, the four U-H homolytic bond strengths, and the electron affinities of the four possible fragment radicals. We confirm earlier work that the most acidic site in uracil is at the N1 site; this site is where uracil becomes covalently bonded to a carbon of the ribose sugar in RNA. G3 calculations for the N1 site at 298 K give $\Delta H^{\circ}_{\text{acid}}(\text{uracil}) = 334.5 \text{ kcal mol}^{-1}$ and $\Delta G^{\circ}_{\text{acid}}(\text{uracil}) = 327.1 \text{ kcal mol}^{-1}$ at 298 K, in good agreement with the experiment. The weakest H-atom bond enthalpy (at the N1 site) is calculated to be $101.8 \text{ kcal mol}^{-1}$.

2.6. Electron Attachment to Cl₂ from 300 to 1100 K

Rate constants for dissociative electron attachment to Cl₂ have been measured from 300 to 1100 K in a high-temperature flowing-afterglow Langmuir-probe apparatus. *R*-matrix calculations have been carried out which compare well with the present measurements with possible deviation at the highest temperatures. The attachment rate constants do not show Arrhenius behavior. The temperature dependence of the calculated rate constants for successive vibrational levels provides insight as to this behavior. While the lowest vibrational level of Cl₂ dominates attachment at low temperatures, the rate constant is not flat with temperature because of the *p*-wave character of the attachment process. The non-Arrhenius behavior is due to a conflict between the increase in attachment cross section with vibrational level (temperature) and the decline in the cross section with electron energy above 50meV.

2.7. Electron Attachment and Detachment

Measurements are reported of rate constants for electron attachment to C₆F₅X (X=Cl,Br,I) and thermal electron detachment from C₆F₅Cl⁻ over the temperature range 300–550 K in 133 Pa of He gas in a flowing-afterglow Langmuir-probe apparatus. This is the first case we know of where the parent anion has sufficiently low electron detachment energy that detachment (from C₆F₅Cl⁻ in this case) has been observed in competition with a channel for dissociative electron attachment yielding a thermally stable anion (here, Cl⁻). Because of this competition, it is shown that a simple mass spectrometric determination of the product branching fractions at long times will lead to erroneous results at elevated temperatures. The electron density profiles provide evidence for a new plasma decay process involving the detaching and nondetaching anions trapped in the space charge field of the positive ions. Electron attachment rate constants were found to be 1.0×10^{-7} , 1.1×10^{-7} , and $2.0 \times 10^{-7} \text{ cm}^3 \text{ s}^{-1}$, at 300 K, for C₆F₅Cl, C₆F₅Br, and C₆F₅I, respectively, estimated accurate to $\pm 25\%$ except for C₆F₅I, where there is $\pm 30\%$ uncertainty. Rate constants for C₆F₅Cl changed little over our temperature range, while those for C₆F₅Br, and C₆F₅I increased with temperature. Electron detachment occurred only for C₆F₅Cl⁻ in our temperature range. Detachment rate

constants were immeasurable at room temperature but approached 4000 s^{-1} at 550 K. From these data the electron affinity (EA) for C6F5Cl was determined, EA (C6F5Cl)= 0.75 ± 0.08 eV. G3(MP2) calculations (based on Møller-Plesset perturbation theory) were carried out for the neutral and anion and yielded EA(C6F5Cl)= 0.728 eV.

2.8. Strong Emission from CaO in the 500 to 900 nm Region

Research revealed some interesting spectral data which showed strong emission from CaO in the 500 to 900 nm region. The purpose of this section is to document the procedure that was used to make a rough prediction of these spectra.

The spectra of particular interest are generated by the vibration-rotation transitions from the $A^1\Sigma$ electronic state to the $X^1\Sigma$ ground electronic state. Because the anharmonicity of the vibrational sublevels of these electronic states is relatively small, these spectra are grouped into bands corresponding to the vibrational quantum number change.¹ The anharmonicity leads to a “blurring” of the band heads. The rotational spreading of the bands is toward the red.

An example of these spectra is shown for a re-entry object in Figure 1. The peaks at the right of the figure are labeled with the change in vibration quantum number during the transition. Peaks are easily seen for $\Delta v = 0, 1, 2$ and 3. There are weaker transitions from a lower lying, A'^1P , electronic state to the ground state which complicate this spectrum^{2, 3} under some conditions, but they are not of interest to this study. The spectra labeled green and orange are complex spectra originating primarily from higher electronic states of CaO.⁴⁻⁷

The dashed line in the figure is representative of a black body curve at 1750 K. This is representative of a solid surface radiating at the temperature. The spectrum has been transmitted through a large atmospheric path and thus shows the oxygen “atmospheric” band absorption at 7600 and 6900 Å. The usual sodium radiation at 5900 Å is also expected.

A computation of the spectrum is made using estimates for the CaO concentration and temperature. The CaO radiator is expected to be in the gas phase boundary layer of the re-entry object. To first order, the radiator thickness is not important. The temperature is used to compute the density of the radiating state from the CaO concentration. The radiation is then computed from the usual equation for molecular radiation from diatomic gases.^{8, 9}

The computation of the spectrum requires the Einstein coefficient (inverse lifetime) of each of the vibrational transitions. These lifetimes have been measured for many molecules but not for CaO. There are only limited measurements and calculation of some of the transitions. The Einstein coefficients will then be estimated by computation of Franck-Condon factors in the usual manner.¹⁰ The Einstein coefficient is proportional to the cube of the transition frequency times the Franck-Condon factor times the electronic transition moment. The electronic transition moment must be estimated.

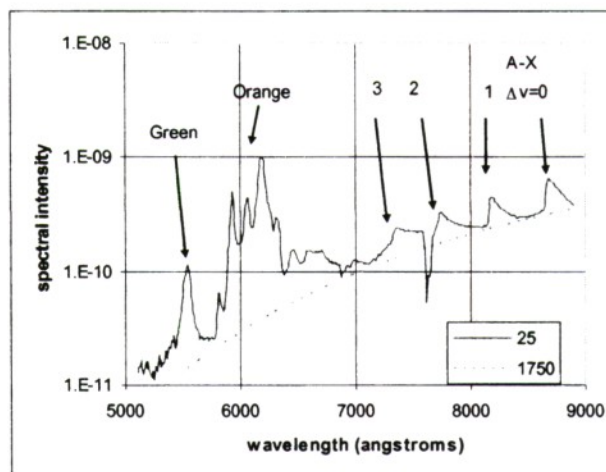


Figure 1. Emission Spectrum of Interest

The computation of the Franck-Condon factors requires information on the potential functions. These are found from the spectroscopic constants for the molecular states. The spectroscopic constants used are given in Table 1. The potential functions are then used in the Schrodinger equation to find the vibrational transition moments and thus the Franck-Condon factors and r-centroids.

Table 1. Spectroscopic Constants^{1, 11, 12} for CaO

	Te	we	wexe	weye	Be	alpha	De	D0
A	11554.8	718.9	2.11		0.40592	0.00137	5.4E-7	37400
X	0	732.03	4.8307	0.00887	0.44444	0.003282	6.5E-7	48350

The Franck-Condon factors and r-centroids were computed with the assistance of the codes provided by Le Roy.¹³ The Franck-Condon factors and r-centroids were found to be acceptably close to limited available literature values.¹⁴⁻¹⁶

The values of the electronic transition moments were then evaluated by comparison with available lifetime estimates. Irwin and Dagdigian¹⁷ estimated the lifetime of the A¹Σv'(v=6) state as 155±60 ns. Diffenderfer and Yarkanoy¹⁸ computed this lifetime to be 130 ns. Plane and Nien¹⁵ measured the lifetime of the radiation from the A¹Σv'(v≤2) states as 150 ns. Thus, we have taken the sum of the Einstein coefficients of each of the upper vibrational levels to be equal to 7 μs⁻¹ (each of these states having the same electronic transition moment). The individual values are given in Table 2.

There is a reference¹⁹ to an unpublished evaluation of the variation of this electronic transition moment with r-centroid, constant*exp(-3.58*r_{v,v'}). However, this did not give results consistent with the lifetime measurements.

Table 2. Einstein Coefficients for $A^1\Sigma(v') \rightarrow X^1\Sigma(v'')$, μs^{-1}

$v' \setminus v''$	0	1	2	3	4	5	6	7	8	9	10
0	3.504	2.680	0.734	0.080	0.003						
1	3.125	0.141	2.213	1.302	0.210	0.008					
2	1.717	1.820	0.184	1.318	1.593	0.352	0.015				
3	0.722	2.172	0.602	0.654	0.664	1.692	0.476	0.019			
4	0.254	1.425	1.772	0.080	0.903	0.291	1.677	0.578	0.021		
5	0.086	0.680	1.761	1.143	0.009	0.920	0.104	1.625	0.651	0.018	0.003
6	0.022	0.273	1.112	1.739	0.614	0.138	0.800	0.028	1.561	0.698	0.015
7	0.005	0.099	0.531	1.421	1.512	0.259	0.299	0.657	0.006	1.526	0.686
8	0.002	0.030	0.257	0.967	1.854	1.404	0.084	0.049	0.590		1.762
9		0.009	0.099	0.541	1.541	2.287	1.257	0.010	0.733	0.522	
10		0.002	0.026	0.196	0.792	1.816	2.133	0.876	0.007	0.783	0.368

The spectral radiation was computed^{20, 21} for a re-entry object at 25 km, observed at 10 km from a distance of about 250 km. The surface temperature was taken as 1750 K and the concentration and temperature of CaO varied. The result is shown in Figure 2 for a temperature of 2500K, a Na concentration of 1 ppm, and a CaO concentration of 20 ppm.

The proper evaluation of this radiation requires detailed object definition, trajectory, ablation and flow-field calculations. The purpose here is to show document the procedure, to the result and to demonstrate the capability.

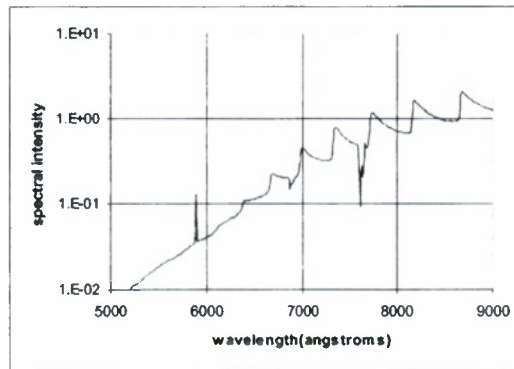


Figure 2. Spectral Radiation for a Reentry Object at 25km

3. SPACE CHEMISTRY

The application of chemical techniques to the development of new technologies for Air Force space-based systems and related issues were also addressed under this contract. These techniques were pursued in the prime interest of enabling space-based systems to be miniaturized down to the pico-satellite regime (<1kg).

Research efforts in support of this topic were towards the development of a miniaturized, satellite skin sensor technology capable of measuring ionospheric neutral particle densities. This real-time, in-situ capability enables the concept of distributed, remote

density measurements, via pico-satellites, to provide 3-dimensional mapping of ionospheric phenomena relevant to space weather forecasting software such as AF-GEOSpace. In addition, for distributed pico-satellite systems that require precision formation flying, this same sensor technology would enable on-line orbital drag evaluation, to allow for accurate station keeping.

All aspects of the research were supported including data acquisition, data analysis, equipment maintenance and upgrade designs. All data sets were delivered to AFRL as they became available. In addition, day-to-day operations of the AFRL/RVBXT space chemistry laboratory were addressed under this contract. This included the oversight of the chemical inventory and hazardous waste accumulation. Results of our research were presented at national and international conferences and published in peer reviewed journals. Section 6 lists five publications that resulted from our efforts under this contract.

Some of the more notable research results are summarized in the following sections. The investigations described were conducted at the AFRL/RVBXT facilities. These facilities include a state-of-the-art Space Chemistry Lab guided-ion beam instrument, and a similar modular system designed for simple modifications of the basic ion beam experiment.

3.1. A Guided-Ion Beam Study of the $O^+(^4S) + NH_3$ System

We measured absolute cross section for the reaction of ground-state O^+ with ammonia at collision energies in the range from near-thermal to approximately 15 eV, using the guided-ion beam (GIB) method. Measurements were also performed using ammonia- d_3 to aid in mass assignments. The reaction is dominated at low collision energies by charge transfer; however, the cross section for this exothermic channel is rather small, decreasing sharply with energy from $\sim 40 \text{ \AA}^2$ for normal ammonia at near-thermal energies and leveling off at 3.7 \AA^2 above 6 eV; the cross section is slightly smaller for ammonia- d_3 . Other channels, corresponding to the production of NH_2^+ and NO^+ , and possibly OH^+ , were detected. The NO^+ channel, although nominally exothermic, is very small and exhibits a threshold at ~ 7 eV. Product recoil velocity distributions were also determined at selected collision energies, using GIB time-of-flight methods.

3.2. Reactions of O^+ with C_nH_{2n+2} , $n = 2-4$: A Guided-Ion Beam Study

We measured absolute reaction cross sections for the interaction of O^+ with ethane, propane, and n -butane at collision energies in the range from near thermal to approximately 20 eV, using the guided-ion beam (GIB) technique. We have also measured product recoil velocity distributions using the GIB time-of-flight (TOF) technique for several product ions at a series of collision energies. The total cross sections for each alkane are in excess of 100 \AA^2 at energies below ~ 2 eV, and in each case several ionic products arise. The large cross sections suggest reactions that are dominated by large impact parameter collisions, as is consistent with a scenario in which the many products derive from a near-resonant, dissociative charge-transfer process that leads to several fragmentation pathways. The recoil velocities, which indicate product ions with largely thermal velocity distributions, support this picture. Several product ions, most notably the C_2H_3-1 fragment for each of the alkanes, exhibit enhanced reaction efficiency as collision energy increases, which can be largely attributed to endothermic channels within the dissociative charge transfer mechanism.

3.3. Hyperthermal Reactions of $O^+(^4S_{3/2})$ with CD_4 and CH_4

Theoretical and experimental methods were applied to the study of the reaction dynamics in hyperthermal collisions of $O^+(^4S_{3/2})$ with methane. Measurements of the absolute reaction cross sections for the interaction of O^+ with CD_4 and CH_4 were obtained at collision energies in the range from near-thermal to approximately 15 eV, using the guided-ion beam (GIB) technique. Product recoil velocity distributions, using the GIB time-of-flight (TOF) methods, were determined for several product ions at selected collision energies. The main reaction channel, charge transfer, proceeds via large impact parameter collisions. A number of minor channels, involving more intimate collisions, were also detected. Ab initio electronic structure calculations have been performed with different levels of theory and basis sets, including high-level coupled-cluster calculations to determine the energies of reaction intermediates and transition states for reaction. Several reaction paths on both quartet and doublet electronic states of $(O-CH_4)^+$ are found, and these provide a reasonable qualitative interpretation of the experiments. Although most of the products can be produced via spin-allowed pathways, the appearance of CH_3^+ at low energies suggests that intersystem crossing plays some role.

4. SMEI SUPPORT AND INTERPLANETARY RESEARCH

One of the goals of our research efforts on this contract was to work toward understanding the origins and interplanetary propagation (IP) of disturbances that affect the geosphere, and to support and analyze the data from the AFRL/NASA Solar Mass Ejection Imager (SMEI) experiment which was launched on the Coriolis spacecraft in January 2003. Our research utilized pertinent satellite and ground-observations of solar, IP and geomagnetic phenomena and, in particular, the new observations from the unique SMEI experiment.

Our studies involved both historical and new data acquired over the course of this contract. It primarily addressed three general topics including:

- the solar eruptive phenomena which lead to sporadic geomagnetic storms
- IP shocks and other signatures of solar ejecta
- the characteristics of IP disturbances which produce geomagnetic storms

The primary results of our research were presented in numerous conferences nationally and internationally. Two papers directly related to the work performed under this contract were published in peer-reviewed journals. They are included in Section 6.0. The most relevant research efforts are summarized in the following sections.

4.1. Major Geomagnetic Storms

Seventy-nine major geomagnetic storms (minimum $Dst \leq -100$ nT) observed in 1996 to 2004 were the focus of a “Living with a Star” Coordinated Data Analysis Workshop (CDAW) in March 2005. In nine cases, the storm driver appears to have been purely a corotating interaction region (CIR) without any contribution from coronal mass ejection-related material (interplanetary coronal mass ejections (ICMEs)). These storms were generated by structures within CIRs located both before and/or after the stream interface that included persistently southward magnetic fields for intervals of several hours. We compare

their geomagnetic effects with those of 159 CIRs observed during 1996–2005. The major storms form the extreme tail of a continuous distribution of CIR geoeffectiveness which peaks at $Dst = -40$ nT but is subject to a prominent seasonal variation of ± 40 nT which is ordered by the spring and fall equinoxes and the solar wind magnetic field direction toward or away from the Sun. The O'Brien and McPherron (2000) equations, which estimate Dst by integrating the incident solar wind electric field and incorporating a ring current loss term, largely account for the variation in storm size. They tend to underestimate the size of the larger CIR-associated storms by $Dst = 20$ nT. This suggests that injection into the ring current may be more efficient than expected in such storms. Four of the nine major storms in 1996–2004 occurred during a period of less than three solar rotations in September to November 2002, also the time of maximum mean IMF and solar magnetic field intensity during the current solar cycle. The maximum CIR-storm strength found in our sample of events, plus additional 23 probable CIR-associated $Dst \leq -100$ nT storms in 1972–1995, is ($Dst = -161$ nT). This is consistent with the maximum storm strength ($Dst = -180$ nT) expected from the O'Brien and McPherron equations for the typical range of solar wind electric fields associated with CIRs. This suggests that CIRs alone are unlikely to generate geomagnetic storms that exceed these levels.

4.2. Solar Mass Ejection Imager (SMEI) Observations of CMEs

The Solar Mass Ejection Imager (SMEI) on the Coriolis spacecraft has been obtaining white light images of nearly the full sky every 102 minutes for three years. We present statistical results of analysis of the SMEI observations of coronal mass ejections (CMEs) traveling through the inner heliosphere; 139 CMEs were observed during the first 1.5 years of operations. At least 30 of these CMEs were observed by SMEI to propagate out to 1 AU and beyond and were associated with major geomagnetic storms at Earth. Most of these were observed as frontside halo events by the SOHO LASCO coronagraphs.

5. DEFENSE METEOROLOGICAL SATELLITE PROGRAM (DMSP)

Our efforts in support of DMSP research included the development of a time history data base. This data base includes measurements of the early DMSP vehicles F13, F14 and F15 together with the measurements made by DMSP vehicles F16 and F17, launched during the course of this contract. These databases have been essential to the generation of data products of AFRL/RVBX use as well as space weather applications at other government facilities such as the Air Force Weather Agency (AFWA).

5.1. DMSP Data Base Development

The objective of this effort was to maintain the time history databases from the previously flown DMSP vehicles and to continue to develop time history databases for the vehicles launched during the course of this contract.

To date, the data base includes measurements from the DMSP vehicles, F13, F15, F16 and F17. AFWA reported a hardware failure on the F14 recorded on August 23, 2008. Thus

no data was received for F14 after this date. The tasks inherent in the development of this database are described in this section of the report.

AFWA redesigned the DMSP mission sensor satellite data files, known as PREP files, into Raw Sensor Data Record (RSDR) files. The new format replaced the 36-bit processed files, containing sensor and file structure specific information, with a standard 32-bit format containing only sensor specific information. Boston College efforts included modifying pre-developed software to transform the RSDR files into time-ordered databases. This software reads the RSDR files and generates SSJ/4, SSIES and SSM time-ordered databases. Boston College personnel run the software and provide quality control checks on a daily basis.

Each RSDR file contains one payload of sensor data. Instead of receiving twelve hours of data bundled, each payload is received soon after it is processed. Calculated ephemeris data, time codes, and on-board ephemeris are provided for each second of data rather than for each minute. This time and ephemeris information is identical for specific DMSP flights. Each 36-bit sensor data word is divided into three, 12-bit words and stored right justified in a 16-bit word. However, the RSDR file does not contain the year and day associated with the sensor data. The year and day must be calculated by the use of a set of subroutines that assume that a given time and its associated ephemeris are accurate and that the day given is the day of data or a day within the past three or four days. Each RSDR file will have a name to uniquely identify the data set. The file name will contain the satellite designation, playback revolution number, the year, day, hour, and minute that the RSDR was created, and the sensor identification.

The new Phase 1 time history database formats contain only 16-bit or 32-bit integer data and 8-bit ASCII characters. Each 9-bit data sensor value is stored right justified in a 16-bit word. Each block of data contains one minute of data.

DMSP data, stored in RSDR format, is transformed into time-ordered databases on a UNIX workstation. Raw data sets for the SSJ, SSIES, and SSM are acquired, copied, and archived.

Input data is copied by using Secure File Transfer Protocol (SFTP) between the computer at Offutt AFB and the Amber, a SUN Microsystems UNIX computer. To automate this procedure a script is executed at designated times during the day to acquire these files. For each experiment, for each vehicle, a multi-day period is stored on UniTree on a daily basis and is also backed up on DVD's on a monthly basis.

Computer modules, written in FORTRAN, with the input data in RSDR format, were carefully developed to generate SSJ, SSIES, and SSM time-ordered databases. Data values are stored in raw counts for each second; ephemeris values are stored at each even minute. A common software package that computes geomagnetic parameters is used for each experiment. A subroutine was written to unpack the three, 12-bit "data" words and convert them to four, 9-bit sensor words. Since any one revolution will neither start nor end exactly at the start or end of a day, care must be taken to ensure that the set of files used as input for one day overlap into the preceding and succeeding days.

To facilitate the creation of a database, script files were written for each experiment that generate a procedure that process multiple days of data that consist of multiple input files. As the script procedure is executed a log file is created that contains processing times and error indications. Directories for each experiment are created. A listing of any directory contains the name, size, and date created of each individual file processed. If the file size for a day of data is not what is expected for a particular experiment, it will be verified that the input data is

unavailable or the error will be found and the day processed again. The database for each day is stored on the UniTree. Copies of the SSJ database files are sent on a daily basis via FTP to Three outside agencies. Copies of the SSIES, SSJ and SSM database files are also archived on to DVD's on a monthly basis.

5.1.1. RSDR SSIES2 Phase II Processing

The Phase II processing system accesses the Phase I time history database. This system is comprised of several software routines coded in FORTRAN and is driven by a UNIX script. Telemetry data values from the Driftmeter (DM), Scintillation Monitor (SM), Retarding Potential Analyzer (RPA), Langmuir Probe (LP) and Microprocessor (MP) experiments are converted into geophysical parameters and written to output files at one-minute intervals. The automated processing is done on a daily basis with a crontab job initiating the shell script at a specified time in the morning. The files are archived on the UniTree file system. Copies of the Phase II data base files are sent on a daily basis via FTP to two outside agencies.

5.1.2. RSDR SSIES2 and SSIES3 Phase II EDR Processing

The processing consists of accessing the phase I files, converting the files to RSDR format, then to EDR data files. The EDR files are compressed and then archived to the UniTree file system.

A copy of the compressed file is also transferred to the FTP server (dropbox) so that the Naval Research Laboratory can retrieve the files via FTP and to FTP servers at NGDC and the Aerospace Corporation.

The processing is done by a combination of UNIX shell scripts, Perl scripts and FORTRAN programs. The automated processing is done on a daily basis with a crontab job initiating the shell script at a specified time in the morning.

5.1.3. RSDR SSM Phase II MFR Processing

The processing consists of accessing the phase I files, converting the files to RSDR format, then to MFR (ASCII) data files. Another program is run converting the ASCII files to binary, the binary files are compressed then transferred to FTP servers at JHU/APL, NGDC and the Aerospace Corporation. Both types of files are also archived to the Unitree file system. The processing is done by a combination of UNIX shell scripts, Perl scripts and FORTRAN programs. The automated processing is done on a daily basis with a crontab job initiating the shell script at a specified time in the morning.

5.1.4. DMSP3 and SWX Web Survey Plot Files (SSIES, SSJ & SSM)

The DMSP3 processing consists of a shell script that accesses input files from Unitree, then runs IDL programs that generate High and Low Latitude data survey plot files. The plots files are copied to the Web server for users to access inside the firewall. The automated processing is done on a daily basis with a crontab job initiating the shell script at a specified time in the morning. The High latitude web plots include SSJ Ion and Electron; SSIES Ni and

N [O+], Horizontal and vertical drift of thermal ions, and SSM measured minus model magnetic field data. The Low latitude web plots include SSIES Ni/N[O+], Ion Drift meter, Temperature and SM total Ion density survey data. Another script, also initiated by a crontab job is run on SWX that copies the plots files generated on dmsp3 on to the SWX web server with a two day delay for users to access outside of the firewall. The log files and web pages are viewed on a daily basis to check for errors in processing

5.1.5. Raw Sensor Data Record Files (RSDR)

RSDR files for SSM, SSIES and SSJ for the period of August 1 through October 31, 2008 were acquired from AFWA for vehicles F13, F15, F16 and F17 (The F14 recorder failed on August 23). AFWA had numerous problems during this reporting period including missing files, corrupted data, especially at the transition of one day to the next and repeating rev readouts that also contained bad data. The problems were reported to AFWA. Many days included some missing files. In some cases they were able to recover the missing files. When missing files were recovered, all of the follow-on programs for the affected data were rerun.

SSJ, SSIES and SSM Time History database files which use RSDR files as input have been generated for the period of August 1 through October 31, 2008. SSIES Phase II database files which use THDB files as input have also been generated for the above time period for vehicles F13 and F15.

SSIES2/3 F13, F15, F16 and F17 EDR Phase II files were processed from August 1 through October 31, 2008. A request by the program manager to run the SSIES2/3 Phase II EDR program with the option to create 24 samples per second files of SM output was completed for the period of July 14-28 2008. A UNIX script was written to process the data further listing only time and density values.

SSM Phase II MFR processing was completed from August 1 – October 31 2008. SSIES, SSJ and SSM Time History database files, SSIES Phase II database files, SSIES EDR, SSM MFR and Ephemeris files have been archived onto DVD's from July 1 - September 30 2008. Two copies of the archive DVD's were made and sent to outside agencies.

RSDR raw files for SSJ, SSIES and SSM were archived onto DVD's for the period of July 1 through September 30, 2008.

DMSP3 Web server plot files were generated for the period of August 1 through October 31. The plot files were copied to the SWX web server through October 29. An anomaly was reported to the program manager pertaining to the F15 Low Lat SM ION density survey plots. The problem started on September 10. It was determined that that the instrument may need to be reset. Also the programmer responsible for the SSIES EDR codes made updates to the codes so the F15 EDR data from September to current will need to be rerun.

5.2. DMSP J4/J5 Data Management

Boston College maintained a complete archive of all DMSP J data from 1983 through the present, beginning with the F6 data and continuous through the currently active DMSP satellites (F13, F15, F16 and F17). This archive is maintained with triple redundancy on a central AFRL/RV file system with a fourth copy of CD. This archive has been made available to all AFRL personnel. In addition, several levels of processed summary data files

are maintained along with viewing software in support of various AFRL projects. Boston College personnel use the archive, processed files and software tools to monitor the status of J instruments on currently active DMSP satellites.

The archive process has been fully automated, but requires manual processing whenever network problems interrupt the automation string, which occurs on most weekends. In addition, log files were routinely monitored for quality control.

During this contract period, the processing software has undergone several updates and viewing software has been upgraded for more rapid use on newer computers.

5.3. DMSP J5 Calibration

Boston College personnel supported the calibration and delivery the J5 instruments for the DMSP program. Calibrations were performed using AFRL's calibration facility for determining detector response to ions and electrons with energies between 100 eV and 20 KeV. The first J5 calibration using this facility was completed in June 2000 and the second in August 2002.

Several serious problems and many minor problems with the calibration facility hardware and software were detected during the initial J5 calibration. Since then, new motors and motor controllers with standard drivers were installed and a Labview user interface was written to replace the existing obsolete calibration software.

Calibration results for the S20 and S16 and S17 were completed and released to the Air Force DMSP program.

Software for the calibration system, CalSys4, was continuously upgraded, debugged, tested and documented. By the end of this contract, a draft user's guide was developed and provided to AFRL.

5.4. DMSP Auroral Boundary Maintenance

Boston College researchers have maintained a random access database of auroral boundaries determined from DMSP J data that is complete from 1982 to the present. The algorithm for determining the auroral boundaries was developed by Boston College personnel. During the course of this contract, we have continued to maintain and upgrade all relevant software. In addition, we have been provided the algorithm and operating system to the Air Weather Service. The boundary data has been used as an indicator for solar activity in their Space Weather Forecasting System.

The bounding algorithm requires six threshold parameters that must be determined for each new DMSP satellite to produce results consistent with the archived boundary data. In addition, yearly updates to the data files have provided. At the close of this contract, routine data processing and data quality control was up to date. In addition, as set of threshold parameters for the AWS boundary algorithm for F16 and F17 was delivered as soon as possible following the successful launch of these vehicles.

5.5. CEASE I and II

The Compact Environmental Anomaly Sensor Experiment (CEASE) consisted of a small environmental hazard detection system that was both lightweight and had low power

requirements. The total package provided data on radiation dose, single event upsets, and charging (spacecraft and dielectric).

A software system has been developed that will take the prime data set, the CEASE Science file, and parse the data into individual time tagged data base files. A program to create an ephemeris time history database from a reconstructed ephemeris file has been written. CEASE was being flown on the Tri-Service Experiments Mission 5 (TSX-5) vehicle that stopped generating data on July 5, 2006. Since the mission was initiated in 2000, the data set is comprised of six years of continuous coverage. Figure 3 illustrates the survey of the > 1 MeV Electrons in an L-shell versus Day for the whole missions.

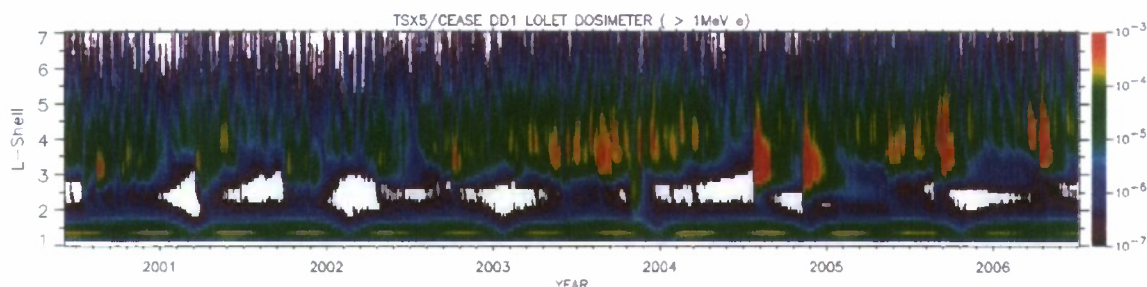


Figure 3. CEASE Measurements from the TSX-5 Vehicle (July 2000-July 2006)

The objective of this project was to generate and maintain the CEASE science and ephemeris databases. This has been achieved and the following describes the contents of the database:

- For the TSX-5 vehicle: CEASE science and ephemeris databases have been generated and cover the time period of Day 160, Year 2000 to Day 186, Year 2006
- For the DSP-21 vehicle, second vehicle equipped with a CEASE sensor: CEASE science and ephemeris databases have been generated and cover the time period of Day 221, Year 2001 to Day 117, 2009.

REFERENCES

1. R. W. Field, *J. Chem. Phys.* **60**, 2400 (1974).
2. R. W. Field, J. A Capelle and C R. Jones, *J. Molec. Spectro.*, **54**, 156 (1975).
3. C. Focsa, A. Poclet, B. Pimchemel, R. J. Le Roy and P. F. Bernath, *J. Molec. Spectro.*, **203**, 330 (2000).
4. D. P. Baldwin and R. W. Field, *J. Molec. Spectro.*, **139**, 77 (1990).
5. D. P. Baldwin and R. W. Field, *J. Molec. Spectro.*, **139**, 68 (1990).
6. D. P. Baldwin and R. W. Field, *J. Molec. Spectro.*, **133**, 90 (1989).
7. Svyatkin, L. A Kuznetsova and U. U. Kuzyakov, *J. Quant. Spectrosc. Radiat. Transfer*, **24**, 25 (1980).

8. Kovacs, *Rotational Structure in the Spectra of Diatomic Molecules*, American Elsevier, 1969.
9. P. Lewis and B. D. Green, *Computation of Electronic Spectra of Diatomic Molecules*, Physical Sciences, Inc., PSI TR-413, 1984.
10. R. J. Spindler, *J. Quant. Spectrosc. Radiat. Transfer*, **4**, 165 (1965).
11. C. E. Blom, H. G. Hedderich, F. J. Lovas, R. D Suenram and A. G. Maki, *J. Molec. Spectro.*, **152**, 109 (1992).
12. <http://webbook.nist.gov/chemistry/>
13. http://leroy.uwaterloo.ca/leroy_programs.html
14. S. N. Suchard, *Spectroscopic Constants for Heteronuclear Diatomic Molecules*, The Aerospace Corporation, Aerospace Report No. Tr-0074(4641)-6, 1974.
15. J. M. C. Plane and C-F Nien, *J. Chem. Soc. Far. Trans.*, **87**, 677 (1991).
16. G. T. Naidu and T. V. R. Rao, *Acta. Phys. Pol.* **A63**, 425 (1983).
17. J. A. Irvin and P. J. Dagdigian, *J. Chem. Phys.*, **74**, 6178 (1981).
18. R. N. Diffenderfer and D. R. Yarkony, *J. Chem. Phys.*, **77**, 5573 (1982).
19. N. E. Kuz'menko, L. A. Kuznetsomva, A. P. Monyakin, Y. Y. Kuzyakov and Y A Plastinin, *Sov. Phys. Usp.*, **22**, 160 (1979).
20. P. Lewis, *RADQCK*, Boston College, AFRL, 2005.
21. M. Eisgruber and E. Sutton, *RADTRAN*, Concord Sciences Corp., 1983.

PUBLICATIONS

J. C. Bopp, T. M. Miller, A. A. Viggiano, and J. Troe, "Experimental and theoretical study of the ion-ion mutual neutralization reactions $\text{Ar}^+ + \text{SF}_n^-$ ($n = 6, 5, \text{ and } 4$)," *J. Chem. Phys.* **129**, 074308 (2008).

J. C. Bopp, J. R. Roscioli, M. A. Johnson, T. M. Miller, A. A. Viggiano, S. M. Villano, S. W. Wren, and W. C. Lineberger, "Spectroscopic characterization of the isolated SF_6^- and C_4F_8^- anions: Observation of very long harmonic progressions in symmetric deformation modes upon photodetachment," *J. Phys. Chem. A* **111**, 1214-1221 (2007).

Y.-H. Chiu, B. L. Austin, R. A. Dressler, D. Levandier, P. T. Murray, P. Lozano, M. M.-Sanchez, "Mass spectrometric analysis of colloid thruster ion emission from selected propellants", *Journal of Propulsion and Power*, **Vol. 21**, 416 (2005).

A. I. Fernandez, I. Dotan, J. F. Friedman, T. M. Miller, J. Troe, and A. A. Viggiano, "Collisional stabilization of highly vibrationally excited *o*-, *m*-, and *p*-xylene ions ($\text{C}_8\text{H}_{10}^+$) from 300 to 900 K and 1 to 250 Torr," *Int. J. Mass Spectrom.* 249-250, **379** (2006).

A. I. Fernandez, A. J. Midey, T. M. Miller, and A. A. Viggiano, "Reaction kinetics of PO_2Cl , PO_2Cl_2^- , POCl_2^- , and POCl_3^- with O_2 and O_3 from 163 to 400 K," *J. Phys. Chem. A.*, **108**, 9120 (2004).

A. Fernandez, A. A. Viggiano, T. M. Miller, S. Williams, I. Dotan, J. V. Seeley, and J. Troe, "Collisional stabilization and thermal dissociation of vibrationally highly excited $\text{C}_9\text{H}_{12}^+$ ions in the reaction $\text{O}_2^+ + \text{C}_9\text{H}_{12} \rightarrow \text{O}_2 + \text{C}_9\text{H}_{12}^+$," *J. Phys. Chem. A*, **108**, 9652 (2004).

J. F. Friedman, T. M. Miller, J. K. Friedman-Schaffer, A. A. Viggiano, G. K. Rekha, and A. E. Stevens, "Electron attachment to $\text{Ni}(\text{PF}_3)_4$ and $\text{Pt}(\text{PF}_3)_4$," *J. Chem. Phys.*, **128**, 104303 (2008).

J. F. Friedman, T. M. Miller, L. C. Schaffer, A. A. Viggiano, and I. I. Fabrikant, "Electron attachment to Cl_2 from 300-1100 K: experiment and theory," *Phys. Rev. A* **79**, 032707 (2009).

J. F. Friedman, A. E. Stevens, T. M. Miller, and Viggiano, A. A., "Electron attachment to MoF_6 , ReF_6 , and WF_6 ; reaction of MoF_6^- with ReF_6 ; and reaction of Ar^+ with MoF_6 ," *J. Chem. Phys.* **124**, 224306 (2006).

B. Gamblin, O. B. Toon, Y. Kondo, N. Takegawa, H. Irie, M. Koike, P. K. Hudson, M. A. Tolbert, J. O. Ballenthin, D. E. Hunton, T. M. Miller, A. A. Viggiano, B. E. Anderson, M. Avery, G. W. Sachse, K. Guenther, C. Sorenson, M. J. Mahoney, "Nitric acid condensation on ice, Part I: Non- HNO_3 Constituent of NO_y Condensing on Low Temperature Upper Tropospheric Cirrus Cloud Particles," *J. Geophys. Res.* **111**, D21203(1-13), (2006).

B. Gamblin, O. B. Toon, M. A. Tolbert, Y. Kondo, N. Takegawa, H. Irie, M. Koike, P. K. Hudson, J. O. Ballenthin, D. E. Hunton, T. M. Miller, A. A. Viggiano, B. E. Anderson, M.

Avery, G. W. Sachse, K. Guenther, C. Sorenson, M. J. Mahoney , “Nitric acid condensation on ice: 2. Kinetic limitations, a possible ‘cloud clock’ for determining cloud parcel lifetime,” *J. Geophys. Res.* **112**, D12209 (2007).

W. Geppert, A. Ehlerding, F. Hellberg, S. Kalhori, R. D. Thomas, O. Novotny, S. T. Arnold, T. M. Miller, A. A. Viggiano, and M. Larsson, “First observation of four-body breakup in electron recombination: $C_2D_5^+$,” *Phys. Rev. Lett.* **93**, 153201 (2004)

H. Gould and T. M. Miller, “Recent developments in the measurement of static electric dipole polarizabilities,” *Adv. At. Mol. Opt. Phys.* **51**, 343-361 (2005).

K. Graupner, L. M. Graham, T. A. Field , C. A. Mayhew, I. I. Fabrikant, T. M. Miller, M. Braun, M.-W. Ruf, and H. Hotop, “Highly-resolved absolute cross sections for dissociative electron attachment to SF_5CF_3 ,” *Int. J. Mass Spectrom.* **277**, 113-122 (2008).

D. J. Levandier, Y. Chiu and R. A. Dressler, “Reactions of O^+ with C_nH_{2n+2} , $n = 2-4$: a guided-ion beam study”, *J. Chem. Phys.*, **120**, p. 6999 (2004).

D.J. Levandier, Y. Chiu, and R.A. Dressler, “A Guided-Ion Beam Study of the $O^+(4S) + NH_3$ System at Hyperthermal Energies, *J. Phys. Chem. A*, **112** (39), pp 9601–9606 (2008).

D. J. Levandier, Y. Chiu, R.A. Dressler, L. Sun, and G.C. Schatz, “Hyperthermal reactions of $O^+(^4S_{3/2})$ with CD_4 and CH_4 : theory and experiment”, *J. Phys. Chem. A*, **108**, pp. 9794-9804 (2004).

A. J. Midey, I. Dotan, S. Lee, W. T. Rawlins, M. A. Johnson and A.A.Viggiano, “Kinetics for the Reactions of O^- and O_2^- with $O_2(a^1\Delta_g)$ Measured in a Selected Ion Flow Tube at 300 K,” *J. Phys. Chem. A* **111**, 5218 (2007).

A. J. Midey, I. Dotan and A.A.Viggiano, “Reactions of $PO_xCl_y^-$ ions with $O_2(a^1\Delta_g)$, H_2O and Cl_2 at 298 K,” *Int. J Mass Spectrom.* **273**, 7 (2008).

A. J. Midey, I. Dotan and A.A.Viggiano, “Temperature Dependences for the Reactions of O^- and O_2^- with $O_2(a^1\Delta_g)$ from 200 - 700 K,” *J. Phys. Chem. A* **112**, 3040 (2008).

A. J. Midey, A. I. Fernandez, A. A. Viggiano, P. Zhang, and K. Morokuma, “Ion Chemistry of NOO^+ ,” *J. Chem. Phys.* **124**, 114313 (2006).

A. J. Midey, T. M. Miller, R. A. Morris, and A. A. Viggiano, “Reactions of $PO_xCl_y^-$ ions with H and H_2 from 298-500 K,” *J. Phys. Chem. A*, **109**, 2559 (2005).

A. J. Midey, T. M. Miller, and A. A. Viggiano, “Kinetics of Ion-Molecule Reactions with 2-Chloroethyl Ethyl Sulfide at 298 K: a Search for CIMS Schemes for Mustard Gas,” *J. Phys. Chem. A* **112**, 10250 (2008).

- A. J. Midey, T. M. Miller, and A. A. Viggiano, "Kinetics of ion-molecule reactions with dimethyl methylphosphonate at 298 K for CIMS detection of GX," *J. Phys. Chem. A* **113**, 4982 (2009). Published online April 23, 2009.
- A. J. Midey, T. M. Miller, and A. A. Viggiano, "Reactions of N^+ , N_2^+ , and N_3^+ with NO from 300 to 1400 K," *J. Chem. Phys.*, **121**, 6822 (2004).
- A. J. Midey and A. A. Viggiano, "Kinetics of Sulfur Oxide, Sulfur Fluoride, and Sulfur Oxyfluoride Anions with Atomic Species at 298 and 500 K," *J. Phys. Chem. A*, **111**, 1852 (2007).
- T. M. Miller, "Thermal electron attachment and detachment in gases," *Adv. At. Mol. Opt. Phys.* **51**, 299-342 (2005).
- T. M. Miller, J. O. Ballenthin, A. A. Viggiano, B. E. Anderson, C. C. Wey, "Mass distribution and concentrations of negative chemiions in the exhaust of a jet engine: sulfuric acid concentrations and observation of particle growth," *Atmos. Environ.* **39**, 3069-3079 (2005).
- T. M. Miller, J. F. Friedman, and A. A. Viggiano, "Electron attachment and detachment, and the electron affinities of isomers of trifluoromethylbenzotrile," *J. Chem. Phys.*, **121**, 9993 (2004)
- T. M. Miller, J. F. Friedman, J. S. Williamson, and A.A. Viggiano, "Rate constants for the reactions of CO_3^- and O_3^- with SO_2 from 300 to 1400 K," *J. Chem. Phys.* **124**, 144305(5), (2006).
- T. M. Miller, J. F. Friedman, J. S. Williamson, L. C. Schaffer, and A. A. Viggiano, "A new instrument for thermal electron attachment at high temperature: NF_3 and CH_3Cl rate constants up to 1100 K," *Rev. Sci. Instrum.* **80**, 034104 (2009).
- T. M. Miller and A. A. Viggiano, "Electron attachment and detachment: C_6F_5Cl , C_6F_5Br , and C_6F_5I , and the electron affinity of C_6F_5Cl ," *Phys. Rev. A*, **71**, 012702 (2005).
- T. M. Miller, A. A. Viggiano, and W. R. Dolbier, T. A. Sergeeva, and J. F. Friedman, "Electron attachment to SF_5 compounds: $SF_5C_6H_5$, $SF_5C_2H_3$, S_2F_{10} , and SF_5Br , 300-550 K", *J. Phys. Chem. A* **111**, 1024-1029 (2007).
- T. M. Miller, A. A. Viggiano, and J. Troe "Electron attachment to SF_6 under well defined conditions: Comparison of statistical modeling results to experiments," *J. Phys. Conf. Series.* **115**, 012019 (2008).
- S. Popovic, A. J. Midey, S. Williams, A. Fernandez, A. A. Viggiano, P. Zhang and K. Morokuma, "Ion-Molecule Rate Constants and Branching Ratios for the Reaction of $N_3^+ + O_2$ from 120 to 1400 K," *J. Chem. Phys.*, **121**, 9481 (2004).

J. C. Poutsma, A. J. Midey, and A. A. Viggiano, "Absolute Rate Coefficients for the reactions of $O_2^- + N(^4S_{3/2})$ and $O_2^- + O(^3P)$ at 298 K in a Selected-Ion Flow Tube Instrument," *J. Chem. Phys.* **124**, 074301 (2006).

I.G. Richardson, et al., Major geomagnetic storms ($Dst \leq -100$ nT) generated by corotating interaction regions, *J. Geophys. Res.*, **111**, A07S09 (2005).

X. N. Tang, H. Xu, T. Zhang, Y. Hou, C. Chang, C. Y. Ng, Y. Chiu, R. A. Dressler and D. J. Levandier, "A pulsed-field ionization photoelectron secondary ion coincidence study of the $H_2^+(X, v^+ = 0-15, N^+ = 1) + He$ proton transfer reaction", *J. Chem. Phys.*, **122**, 164301 (2005).

J. M. Van Doren, J. F. Friedman, T. M. Miller, A. A. Viggiano, S. Denifl, P. Scheier, T. D. Märk, and J. Troe, "Electron attachment to $POCl_3$: Measurement and theoretical analysis of rate constants and branching ratios as a function of gas pressure and temperature, electron temperature, and electron energy," *J. Chem. Phys.* **124**, 124322 (2006).

J. M. Van Doren, S. Williams, A. J. Midey, T. M. Miller, and A. A. Viggiano, "Temperature dependence of the oxide ion/ozone reaction in the gas phase," *Int. J. Mass Spectrom.*, **241**, 185 (2005).

J. M. Van Doren, T. M. Miller, A. A. Viggiano, P. Španěl, D. Smith, J. C. Bopp, and J. Troe, "Experimental investigation of electron attachment to SF_5Cl ," *J. Chem. Phys.* **128**, 094309 (2008).

J. M. Van Doren, T. M. Miller, and A. A. Viggiano, "G3 and density functional theory investigations of the structures and energies of SF_nCl ($n=0-5$) and their anions," *J. Chem. Phys.* **128**, 094310 (2008).

J. M. Van Doren, K. B. Hogan, T. M. Miller, and A. A. Viggiano, "Observation of dihalide elimination upon electron attachment to oxalyl chloride and oxalyl bromide, 300-550 K," *J. Chem. Phys.* **124**, 184313 (2006).

D.F. Webb, et al. Solar Mass Ejection Imager (SMEI) observations of coronal mass ejections (CMEs) in the heliosphere, *J. Geophys. Res.*, **111**, A12101 (2006).

V. Zhaunerchyk, R. D. Thomas, W. D. Geppert, M. Hamberg, M. Kaminska, E. Vigrén, M. Larsson, A. Midey and A. A. Viggiano, "Dissociative Recombination of $OPCl^+$ and $OPCl_2^+$: Pushing the Upper Mass Limit at CRYRING," *J. Chem. Phys.* **128**, 134308 (2008).